Core and Edge Aspects of Quiescent Double Barrier Operation on DIII–D, with Relevance to Critical ITB Physics Issues

E.J. Doyle,[1] T.A. Casper,[2] K.H. Burrell,[3] C.M. Greenfield,[3] W.P. West,[3] R.V. Budny,[4] J.C. DeBoo,[3] A.M. Garofalo,[5] P. Gohil,[3] R.J. Groebner,[3] A.W. Hyatt,[3] G.L. Jackson,[3] T.C. Jernigan,[6] J.E. Kinsey,[7] L.L. Lao,[3] C.J. Lasnier,[2] J.-N. Leboeuf,[8] T.C. Luce,[3] M.A. Makowski,[2] G.R. McKee,[9] R.A. Moyer,[10] M. Murakami,[6] T.H. Osborne,[3] W.A Peebles,[1] C.C. Petty,[3] M. Porkolab,[11] G.D. Porter,[2] T.L. Rhodes,[1] J.C. Rost,[11] D.L. Rudakov,[10] G.M. Staebler,[3] E.J. Strait,[3] M.R. Wade,[6] G. Wang,[1] J.G. Watkins,[12] and L. Zeng[1]

[1]Dept. of Electrical Engineering and PSTI, University of California, Los Angeles, California 90095, USA; email: doyle@fusion.gat.com
[2]Lawrence Livermore National Laboratory, Livermore, California, 94550, USA
[3]General Atomics, P.O. Box 85608, San Diego, California 92186, USA
[4]Princeton Plasma Physics Laboratory, Princeton, New Jersey, 08543, USA
[5]Columbia University , New York, New York 10027, USA
[6]Oak Ridge National Laboratory, Oak Ridge, Tennessee 37381, USA
[7]Lehigh University, Bethlehem, Pennsylvania 18015, USA
[8]Physics Dept., University of California, Los Angeles, California 90095, USA
[9]University of Wisconsin-Madison, Madison, Wisconsin 53706, USA
[10]University of California, San Diego, California 92093, USA
[11]Massachusetts Institute of Technology, Cambridge, Massachusetts 02139, USA
[12]Sandia National Laboratories, Albuquerque, New Mexico 87185, USA

Abstract. Recent results from DIII-D address critical internal transport barrier (ITB) research issues relating to sustainability, impurity accumulation and ITB control, and have also demonstrated successful application of general profile control tools. In addition, substantial progress has been made in understanding the physics of the Quiescent Double Barrier (QDB) regime, increasing the demonstrated operating space for the regime and improving performance. Highlights include: (1) A clear demonstration of q-profile modification using electron cyclotron current drive (ECCD); (2) Successful use of localized profile control using electron cyclotron heating (ECH) or ECCD to reduce central high-Z impurity accumulation associated with density peaking; (3) Theory-based modeling codes are now being used to design experiments; (4) The operating space for Quiescent H-mode (QH-mode) has been substantially broadened, in particular higher density operation has been achieved; (5) Both absolute ($\beta \leq 3.8\%$, neutron rate $S_n \leq 5.5\times10^{15}$ s^{-1}) and relative ($\beta_N H_{89} = 7$ for 10 τ_E) performance has been increased; (6)With regard to sustainment, QDB plasmas have been run for 3.8 s or 26 τ_E. These results emphasize that it is possible to produce sustained high quality H-mode performance with an edge localized mode (ELM)-free edge, directly addressing a major issue in fusion research, of how to ameliorate or eliminate ELM induced pulsed divertor particle and heat loads.

1. Introduction

This paper reports on the progress over the last two years in the areas of Quiescent Double Barrier (QDB) and Quiescent H-mode (QH-mode) research on DIII–D [1-9]. The QDB regime, first reported at the 2000 IAEA Fusion Energy Conference [4], combines internal transport barriers (ITBs) with an edge localized mode (ELM)-free QH-mode edge, resulting in sustained high performance operation with compatible core and edge transport barriers. These QDB discharges are of interest as: (a) QH-mode plasmas demonstrate that sustained, high-quality ELM-free H-mode operation is possible with density and radiated power control, (b) QDB discharges provide a convincing demonstration of quasi-steady-state ITB operation for >3.8 s, or ~26 τ_E, limited by NBI pulse length constraints and, (c) QDB discharges allow us to investigate critical ITB physics issues such as sustainment, edge-core interaction, impurity accumulation, theory-based understanding and current drive capability in enhanced performance discharges.

Progress since the last IAEA conference and relevance to critical ITB research issues can be summarized as follows: (1) *ITB sustainment*; q-profile modification, essential for future

steady-state operation, has been convincingly demonstrated in QDB plasmas using electron cyclotron current drive (ECCD). (2) *Core/edge interaction;* The ELM-free QH-mode edge is a potential solution to the pulsed divertor heat and particle load issues associated with Type I ELM operation in future burning plasmas. The QH-mode edge is also compatible with ITBs. (3) *Understanding*; Theory-based modeling codes are now being used to design ECCD experiments, while characterization of the edge conditions associated with QH-mode operation is much improved. (4) *Profile and impurity control;* Localized profile control using electron cyclotron heating (ECH) or ECCD has been successfully utilized to reduce central high-Z impurity accumulation associated with density peaking. (5) *Operating space;* QH-mode operating space has been substantially broadened, in particular higher density operation has been achieved. (6) *Performance;* Both absolute ($\beta \leq 3.8\%$, neutron rate $S_n \leq 5.5\times10^{15}$ s^{-1}) and relative ($\beta_N H_{89} = 7$ for 10 τ_E) performance has been increased. (7) *Transferability;* In addition to the work on DIII-D, QH-mode has recently been obtained on ASDEX-U [10], demonstrating that this regime is not machine specific.

The operational conditions required to date to access QH–mode/QDB operation can be summarized as follows [1,3,5,7]: (a) Use of counter-neutral beam injection (NBI), (injection anti-parallel to the plasma current), (b) divertor cryopumping to control the density and, (c) a larger than usual gap between the plasma edge and the outer wall (low field side) of ~10 cm. This latter requirement is probably related to the different edge fast ion orbits associated with counter- NBI, and a larger gap is required to prevent ions from interacting with the wall. The structure of the remainder of this paper is as follows: in Section 2 core aspects of QDB operation are considered, edge aspects are discussed in Section 3, while a summary is presented in Section 4. Due to space limitations some topics have had to be omitted from this paper, including a discussion of outstanding issues. Readers are referred to the references for a discussion of why we do not believe counter-NBI is essential in forming QDB plasmas (balanced NBI might also work) [2,6], and for a discussion of potential causes for the ELM suppression observed in QH-mode plasmas (the fundamental reason for ELM suppression has yet to be established) [1,3,7].

2. Core Aspects of Quiescent Double Barrier Operation

An example of the time evolution of a long-pulse, high performance QDB discharge is shown in Fig. 1. The plasma makes a transition to H–mode shortly after counter-NBI heating is applied at 0.8 s. After an initial ELMing phase the discharge evolves into a quiescent phase (QH–mode), as marked by the disappearance of bursts on the D_α emission. During this quiescent phase the line average density and radiated power become essentially constant, indicating that edge particle transport is sufficiently large for divertor cryopumping to control the density and low-Z impurity content. Also during the QH–mode phase, a continuous oscillation is shown on magnetic probe signals after the ELMs cease, Fig. 1(c). This is the edge harmonic oscillation (EHO), which is discussed in Section 3 below. This plasma maintains a quiescent edge for 3.8 s, or ~26 τ_E, and achieves a $\beta_N H_{89}$ product of 6. The quasi-steady state nature of this discharge is evident from the almost constant line average density, central and edge pedestal T_i, and radiated power. However, the q-profile is still evolving, Fig. 1(f), indicating the need for q-profile control in order to achieve true steady-state conditions. Experiments in 2002 concentrated on providing a first demonstration of the ability to modify the q-profile in QDB discharges using the ~2 MW of power available for ECCD. In order to maximize the impact of the available electron cyclotron (EC) power, extensive theory-based current drive simulations were performed [9] using the Corsica code [11]. The simulations used measured density, Z_{eff} and thermal conductivity profiles from previous QDB plasmas, and added 2.5 MW of EC power. The temperature and current profiles were evolved to make predictions for the perturbed q-profile as a function of time, under the assumption that transport rates remain unchanged. In the Corsica analysis mode utilized with experimental ECCD data, time-dependent measured density, Z_{eff}, and temperature profiles that include the effect of EC heating are used. Using either the transport-evolved (simulation) or measured (analysis) profiles, Corsica's Ohm's law solver determines the evolution of the equilibrium, plasma current drive components, and *q*. In both modes, theory-based models are used to calculate the current drive sources; bootstrap, NBCD and ECCD.

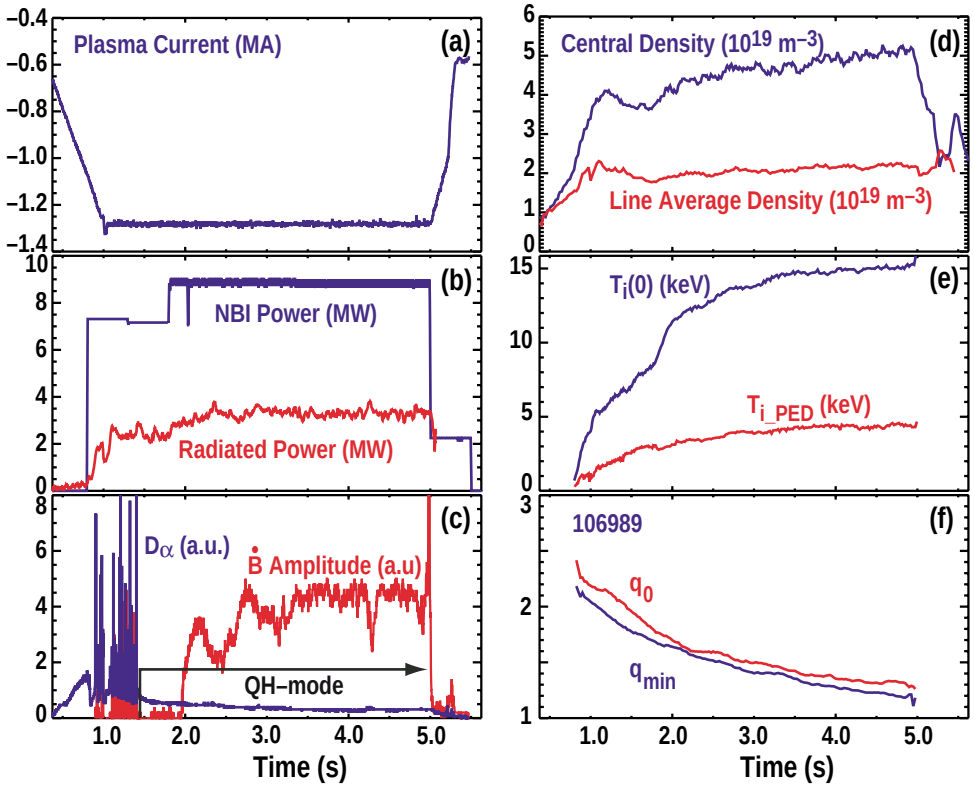

FIG. 1. Time history of a long-pulse QDB plasma (106989), showing: (a) plasma current I_p, (b) P_{NBI} and P_{rad}, (c) divertor D_α emission and magnetic probe signal amplitude, (d) central and line average density, (e) central and edge pedestal T_i and, (f) q_0 and q_{min}. This discharge maintains a quiescent edge for 3.8 s, or ~26 τ_E.

Shown in Fig. 2(a) are the Corsica predictions for the q-profile evolution over a 0.6 s period during injection of 2.5 MW of co-ECCD at ρ ~ 0.35, modeled using measured plasma parameters. As can be seen, the prediction is for significant modification of the q-profile; q_0 to increase and q_{min} to decrease outside of the deposition radius. Shown in Fig. 2(b) is Corsica analysis of results from a corresponding experimental discharge (110874), using ~2 MW of co-ECCD deposited at ρ ~ 0.2-0.3. The plasma conditions for this experiment were 1.3 MA plasma current, 2×10^{19} m^{-3} line average density and 2.0 T toroidal field in an upper single null plasma with divertor cryopumping. Differences between the design simulation and the experiment include a smaller deposition radius in the experiment, which varied in time due to density profile changes, and thermal conductivities changed. Nevertheless, the experimental results are in good qualitative agreement with the design predictions; during the 2.0 s interval in which ECCD is applied in the experiment, q_0 increases initially and then decreases along with decreasing q_{min} outside of the deposition radius. The total ECCD driven current in this case corresponds to ~120 kA. The Corsica analysis shown in Fig. 2(b) is consistent with raw pitch angle data from the motional Stark effect (MSE) diagnostic [12]. As shown in Fig. 3, MSE pitch angle data as a function of radius reflect significant and rapid changes in the current distribution after ECCD application at 2.5 s, and indicate an initial rise in q_0. These results provide a clear demonstration of successful q-profile modification using ECCD in sustained QDB plasmas, as required for sustained ITB operation. The Corsica code has also been used to predict the performance of steady state QDB plasmas with ~6 MW of long pulse EC power [6,9]. Such discharges are predicted to reach a steady state at 40 s, with I_p = –0.79 MA (i.e. reversed I_p, to obtain counter-NBI) and an 80% bootstrap fraction [9].

Pressure profile control is essential in order to realize the full potential of advanced tokamak (AT) plasmas. Such control is needed to tailor ITB location and strength so as to obtain broad pressure profiles, thereby maximizing plasma performance and β limits [4]. In addition, it is well known that impurity transport and accumulation is a major issue for long-pulse high confinement regimes [13]. In particular, density profile peaking associated with ITB operation can lead to central high-Z impurity accumulation. Central high-Z (e.g. nickel and

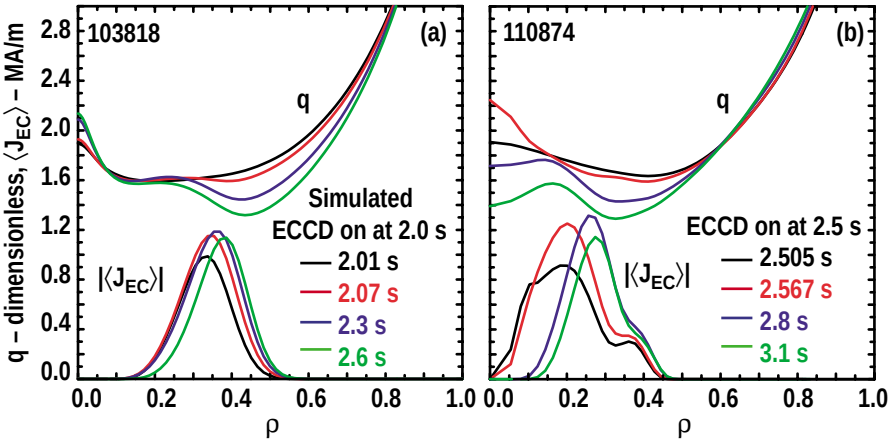

FIG. 2. Shown are: (a) Theory-based design of q-profile control experiment, showing time dependent Corsica simulations of the effect of 2.5 MW of co-ECCD at ρ=0.35, with fixed χ, n_e and Z_{eff} as determined from QDB discharge 103818. (b) Time dependent Corsica analysis of corresponding ECCD experiment, discharge 110874, with ~2 MW of co-ECCD injected at ρ=~0.2-0.3, using experimental time dependent profiles as input.

copper) impurity accumulation is observed in QDB plasmas, which typically have high density peaking factors ($n_e(0)/\bar{n}_e$~2–3) [3,5]. Preliminary 2001 DIII-D experiments demonstrated that ECH injection into existing QDB core barriers substantially broadened the density profile. Similar results have been reported from ASDEX-U [14]. Consequently, a major goal of 2002 experiments was to use this effect to broaden the pressure profile, control density peaking and, hence, reduce preferential central high-Z impurity accumulation.

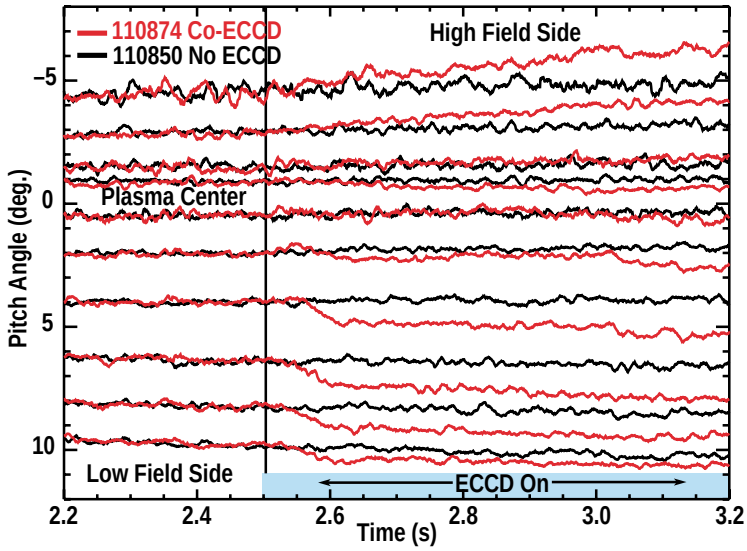

FIG. 3. MSE data for the internal magnetic field pitch angle as a function of radius and time for two discharges, with (110874) and without (110850) ECCD. Channels on the high field side of the device are at the top of the plot while the low field side is at the bottom. The rapid and large changes in pitch angle with ECCD directly indicate q-profile modification, while the data from the central channels indicate an initial transient rise in q_0.

As shown in Fig. 4, DIII-D data clearly demonstrate that ECH/ECCD can provide localized control of profiles and high-Z impurity accumulation. As is apparent from Fig. 4(a), ECCD deposition at ρ ~ 0.2–0.3 leads to a substantial decrease in the density profile peaking factor $n_e(0)/\bar{n}_e$, from ~2.1 before ECCD to ~1.5 after. Similar effects on the density profile are observed with use of ECH or ECCD (both co- and counter). ECH/ECCD deposition at larger radius, ρ ~ 0.4, leads to similar but weaker effects over a broader region. In addition to decreasing the core density, ECH/ECCD also affects other plasma profiles; central T_e increases and T_i decreases. The effect of the ECCD on the total pressure profile is shown in Fig. 4(b), from which it can be seen that the central pressure, and thus beta, is moderately reduced. As shown by Fig. 4(c,d), reduction in the density profile peaking leads to a significant gain with regard to impurity accumulation. Before the application of ECCD the central Z_{eff} is high, ~5, which is reduced to ~4 after ECCD is applied.

The profiles shown were determined from MIST [15] modeling based on spectroscopic data for low- and high-Z impurity species. The individual contributions to Z_{eff} from carbon and

the total high-Z contribution are also shown, from which it is apparent that the reduction in Z_{eff} with ECCD is due to the elimination of the central peaking of the high-Z impurity profiles. It should be noted that counter-NBI operation has historically resulted in higher impurity levels on DIII-D, independent of QDB operation [16]. This demonstration of density profile and high-Z impurity accumulation control in an ITB plasma with moderate impact on plasma performance represents significant progress on a critical ITB physics issue for application to future burning plasmas.

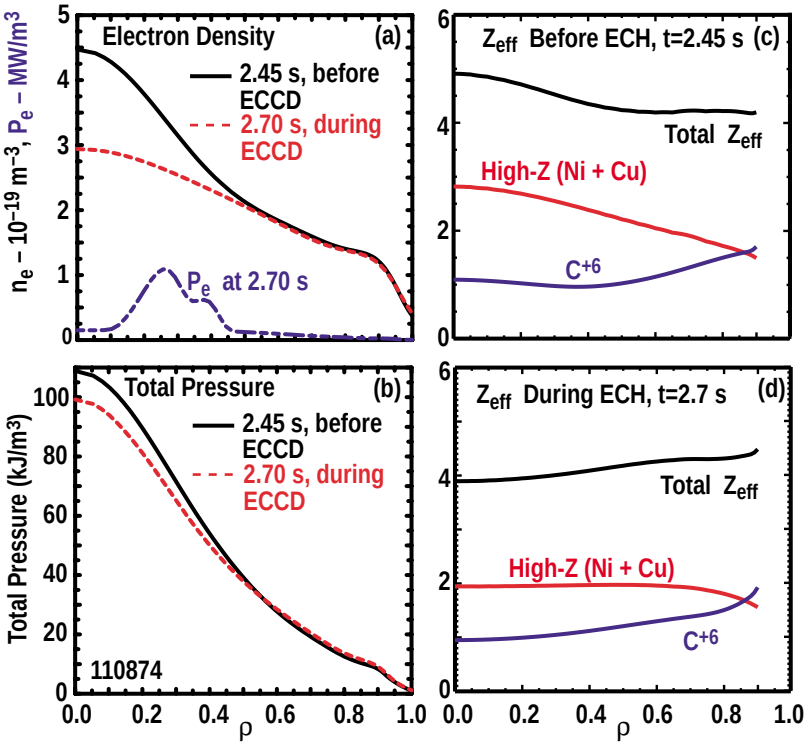

FIG. 4. Showing: (a) density profile before and after ECCD application, with EC deposition profile, (b) total pressure profile before and after ECCD, (c) total Z_{eff} and carbon and high-Z components before ECCD, and, (d) total Z_{eff} and components after ECCD, for discharge 110874.

The transport properties of QDB discharges have been presented in several previous papers, demonstrating the existence of both core and edge transport barriers and showing that core ion thermal diffusivities are reduced to neoclassical levels inside the ITB radius [1-6]. The double transport barriers in QDB plasmas are separated by a null in the E×B shearing rate located between the two barriers [2,6]. Shown in Fig. 5(a) and (b) are T_i and T_e profiles along with TRANSP [17] analysis of thermal diffusivities, Fig. 5(c,d), for discharge 110874, before and after application of ECCD. As can be seen, T_e increases with ECCD (or ECH) application, while T_i decreases. With regard to thermal diffusivities, χ_e is reduced inside the EC deposition radius, while χ_i is increased to above neoclassical levels. Transport modeling of QDB plasmas also has been performed [3,5,6]. However, a serious error was recently discovered [18] in the Shafranov shift stabilization component of the GLF23 transport model [19]. The significance of this error for QDB regime modeling is not yet known; QDB data will be re-analyzed when a corrected version of the model is available.

With regard to turbulence properties, QDB plasmas have some interesting features [3,5,6,20,21]. Neoclassical ion transport levels are obtained with reduced but not entirely suppressed density fluctuation levels. However, reflectometer measurements of the turbulence radial correlation length Δr, indicate a substantial reduction in Δr over a measurement range of $0.1 \le \rho \le 0.4$ in QDB plasmas [3,5,6,20,21]. The reduction is by comparison with previous L–mode measurements, in which Δr was found to scale approximately as 5–10 ρ_s [20,21]. A reduction in the turbulence correlation length should be indicative of a reduction in the step size of the turbulent transport, and is occurring in the region of measured transport reduction. This experimental observation of reduced turbulent correlation lengths in QDB plasmas has been replicated by nonlinear global gyrokinetic modeling of ITG turbulence using the circular-geometry UCAN code [20,21]. Far-infrared scattering data for discharges with ECH/ECCD, such as 110874 discussed above, indicate that core turbulence levels increase by ~20%-30% with application of ECH/ECCD, consistent with the observed increase in ion transport rates. The scattering data also indicate that EC injection has another unanticipated benefit: high frequency (100s of kHz) core Alfvén eigenmode activity frequently observed in these discharges [6] is suppressed within ~100 ms of ECCD initiation. Since such high

frequency Alfvén modes cause enhanced ion redistribution [6], their elimination should aid performance.

The combination of core and edge transport barriers in QDB plasmas results in high core and edge pedestal ion temperatures, $T_i(0) \leq 17$ keV and $T_{i\,PED} \leq 6$ keV, leading to a relatively high fusion reactivity as measured by the DD neutron emission rate, e.g. $S_n \leq 5.5\times10^{15}$ s^{-1} [3]. Since the 2000 IAEA conference both absolute (β, S_n) and relative ($\beta_N H_{89}$, duration) performance has been increased. Relative performance improves with higher input power, while absolute performance improves with increasing I_p and B_T. The highest performance QDB plasma to date (106956) achieves a constant $\beta_N H_{89}$ product of 7 for 1.6 s (10 τ_E), at $I_p = -1.6$ MA, $B_T = -2.0$ T, and $P_{NBI} = 11.8$ MW [3]. Other parameters for this discharge include $T_i(0) = 16$ keV, $\beta_N = 2.7$ %-m-T/MA, $H_{89} = 2.6$, $\beta = 3.8\%$, W = 1.58 MJ, τ_E (total) = 160 ms and DD neutron rate $S_n \leq 5.2\times10^{15}$ s^{-1}. The high performance phase in this discharge was limited in duration by NBI source constraints. In this plasma q_{min} was ~1; QDB plasmas more typically maintain $q_{min} > 1$. Thus, long pulse high performance QDB operation has been maintained even with $q_{min} \sim 1$ and without sawteeth, but with a 1/1 internal mode. The quoted H_{89} factor and confinement times include a correction for prompt beam ion orbit losses, which is typically of the order of 10%.

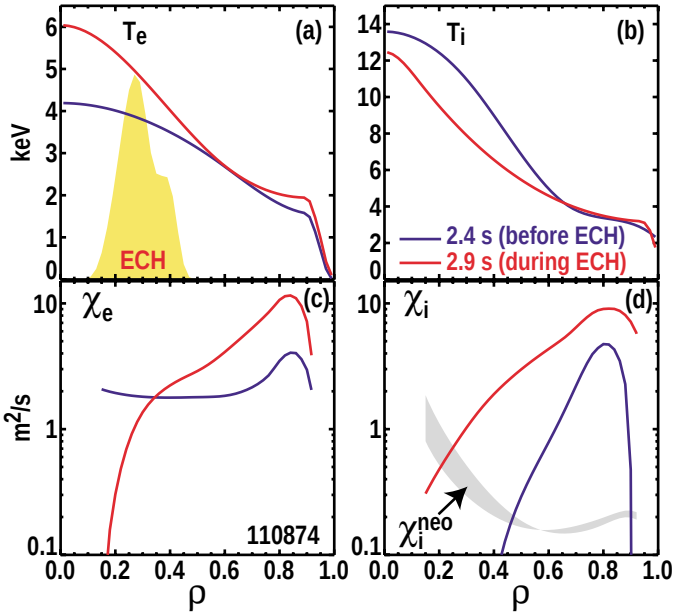

FIG. 5. Profiles of (a) T_e, (b) T_i, (c) χ_e and, (d) χ_i and χ_i neoclassical (thinner lines), for discharge 110874 at two times, 2.45 s (blue curve, before ECCD), and 2.7 s (red curves, during ECCD). Shown as an inset in (a) is the EC power deposition.

3. Edge aspects of QDB operation, the QH-mode edge

The key element in obtaining a QDB discharge is to create a quiescent, ELM-free H–mode edge (QH–mode) [1,3,7,8]. The latter can be obtained without the former, i.e., QH-mode plasmas can be obtained without ITBs. In this section we consider the operating space over which QH-mode has been obtained, edge and divertor conditions and MHD oscillations associated with QH–mode operation. The experimental requirements for obtaining QH–mode were listed in the introductory section, and have been considered in detail in Refs. [1,3,5,7].

QH-mode operating space has been substantially broadened over the last two years. It has been obtained in both upper and lower single-null discharges and across the following parameter range: $1.0 \leq |I_p|$ (MA) ≤ 2.0, $1.8 \leq |B_T|$ (T) ≤ 2.1, triangularity δ of 0.16–0.7 and q_{95} of 3.4–5.8. In addition, we have a low field example at $B_T = -0.95$ T and $I_p = -0.67$ MA. Most work has been performed at $1.2 \leq |I_p|$ (MA) ≤ 1.6, and $\delta \sim 0.4$. In addition, QH–mode has been obtained with both orientations of ∇B with respect to the divertor X-point. To date, QH-mode has only been observed to evolve from standard ELMing or ELM-free H-mode operation, i.e., we have yet to observe a direct transition from L-mode to QH-mode. Consequently, the input power required to obtain QH-mode operation has always been at or above that required for standard H-mode operation. That the QH–mode edge is indeed a true H-mode has been demonstrated in several previous publications [1,3,7]. Figure 6 shows a comparison of edge pedestal conditions in QH–mode with those in Type I and Type III ELMing regimes. It can be seen that much of the QH–mode data occur at low normalized pedestal densities and high T_e. In addition, very high ion pedestal temperatures have been obtained, $T_{i\,PED} \leq 6$ keV. Operation at 2.0 MA plasma current has resulted in higher

QH-mode pedestal densities, as shown by the data point cluster in Fig. 6 at a pedestal Greenwald density fraction of ~0.3. Shown in Fig. 7 is the density profile from a 2.0 MA QH-mode discharge with a line average density of 7.6×10^{19} m^{-3}, corresponding to a Greenwald density fraction $\bar{n}_e/n_{GW} = 0.43$.

The conducted heat flux to the divertor target plates during QH-mode is within typical DIII-D H-mode limits [3,5,8]. An example of the upper divertor heat flux profile as determined from IRTV data is shown in Fig. 8. For this discharge, with 9.3 MW of injected power, the peak measured heat flux is 3.8 MW/m^2 to the inner strike-point. A feature of QH-mode operation is the appearance of an additional peak in the heat flux profile, located on the baffle plate, 4-5 cm outside the separatrix when mapped to the outer midplane [5,8]. This anomalous peak is correlated with the presence of an edge harmonic oscillation (EHO) and is consistent with measurements of a low density population of hot (3-7 keV) carbon ions (C^{+6}) in the scrape-off-layer (SOL) [5,8].

In most cases, QH–mode plasmas are associated with the presence of an EHO [1-3,5-7,22]. As details of the EHO have been published previously, only major points will be presented here. The EHO is continuous during QH–mode operation and is visible on magnetic, density and temperature fluctuation measurements. As its name implies, the EHO typically has multiple harmonics, with toroidal mode numbers ranging from 1 to 10. On DIII–D we have also observed a single example of QDB/QH–mode operation without the EHO, but with a continuous global m=1, n=1 mode which extends to the edge [3,6]. That controlled density, ELM-free H–mode operation can be obtained via a variety of benign MHD activity is encouraging for the robustness and general applicability of these regimes. The EHO is responsible for the ability to maintain density and radiated power control

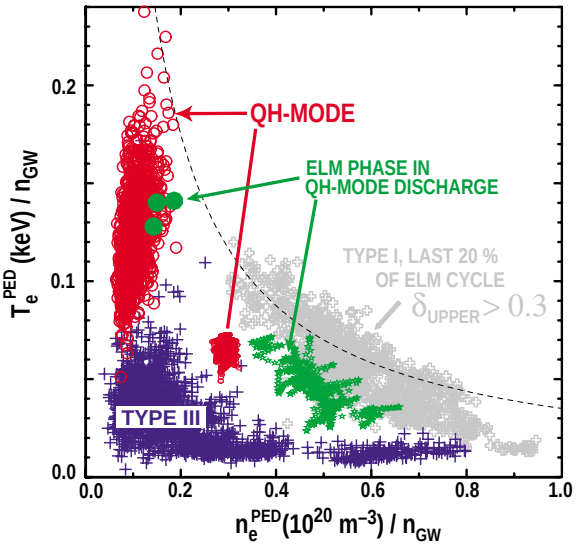

FIG. 6. Comparison of edge pedestal conditions in QH–mode and Type I and III ELMing regimes. The temperature at the top of the pedestal, T_e^{PED} is plotted versus n_e^{PED}, both quantities being determined from Thomson scattering data. Both axes are normalized by the Greenwald density, n_{GW}. The dashed curve illustrates a surface of constant pressure.

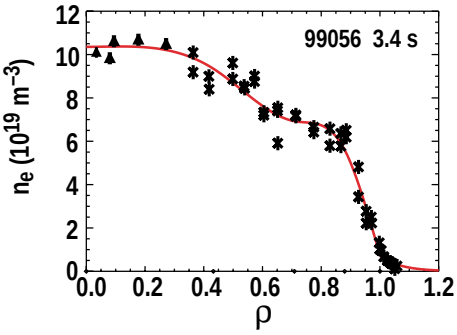

FIG. 7. Density profile for a 2 MA QH-mode discharge (99056), with $n_e^{PED} = 6.5\times10^{19}$ m^{-3} and a line average density of 7.6×10^{19} m^{-3}, corresponding to $\bar{n}_e/n_{GW} = 0.43$.

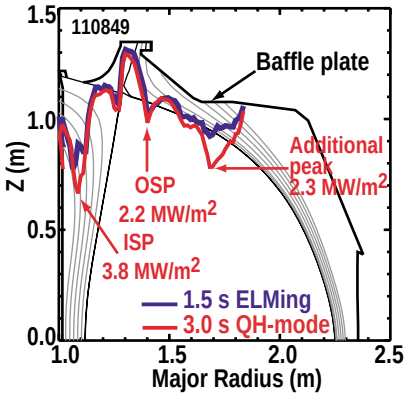

FIG. 8. Measured upper divertor heat flux profile overlaid on a drawing of the DIII-D baffle plate structure. The heat flux is shown for two times during discharge 110849; at 1.5 s (blue curve, 7.2 MW NBI) during the initial ELMing phase of the discharge, and at 3.0 s (red curve, 9.3 MW NBI) during the QH-mode phase. Peak heat fluxes are indicated in the drawing and are 3.8 MW/m^2 to the inner strike-point (ISP), 2.2 MW/m^2 to the outer strike-point (OSP), and 2.3 MW/m^2 to an additional peak located on the outer baffle structure. The line average density for this discharge was 2.2×10^{19} m^{-3}.

in the ELM-free QH–mode regime, by enhancing particle transport in the edge relative to conventional ELM-free operation [1-3,5-7]. Evidence for enhanced transport caused by the EHO include Langmuir probe measurements of ion flux to the divertor strike points [1,3,7]. In addition, the edge density profile at the outer midplane is directly modulated at the fundamental EHO frequency [3,22], while divertor D_α radiation increases at the onset of the EHO, indicating an increased particle flux out of the plasma [1,7]. Results of analysis of edge particle balance and particle pumping in QH-mode are presented in Ref. [5].

In addition to the EHO and very high SOL impurity ion temperatures, one other signature of QH-mode operation should be mentioned. This is the fact that QH-mode operation is associated with a very deep electric field well just inside the separatrix [3,7,8]. An edge E_r well is of course a standard feature of H-mode operation, but the QH-mode well is the deepest seen to date on DIII-D, far exceeding that in comparable conventional ELM-free or ELMing H-mode discharges, or indeed, the ELMing phase of QH-mode discharges.

4. Summary

Substantial progress has been made in increasing understanding of the physics of the QDB regime, broadening its demonstrated operating space and enhancing performance. Highlights include: (1) a clear demonstration of q-profile modification using ECCD, (2) high-Z impurity control in QDB plasmas containing ITBs as a result of ECH/ECCD density profile modification and, (3) attainment of higher density operation. These results both demonstrate the successful application of profile control tools of general utility, and also address critical ITB research issues relating to sustainability, impurity accumulation and ITB profile control. With regard to sustainment, QDB plasmas have been run for 3.8 s or 26 τ_E, while a performance level of $\beta_N H_{89}$=7 has been maintained for 10 τ_E. These results emphasize that it is possible to sustain high quality H-mode performance with an ELM-free edge. This mode of operation offers a solution to a major issue in fusion research, of how to ameliorate or eliminate ELM induced pulsed divertor particle and heat loads.

Acknowledgments

Work supported by U.S. Department of Energy under Grants DE-FG03-01ER54615, DE-FG02-89ER53297, DE-FG02-92ER54141, DE-FG02-89ER53296, DE-FG03-95ER54294, DE-FG02-90ER54084, DE-FG02-94ER54235 APTE, and Contracts W-7405-ENG-48, DE-AC03-99ER54463, DE-AC02-76CH03073, DE-AC05-96OR22725, and DE-AC04-94AL85000.

References

[1] K.H. Burrell, *et al.*, Phys. Plasmas **8**, 2153 (2001).
[2] C.M. Greenfield, et al., Phys. Rev. Lett. **86**, 4544 (2001).
[3] E.J. Doyle, *et al.*, Plasma Phys. Control. Fusion **43**, A95 (2001).
[4] E.J. Doyle, *et al.*, Nucl. Fusion **42**, 333 (2002).
[5] W.P. West, *et al.*, Phys. Plasmas **9**, 1970 (2002).
[6] C.M. Greenfield, *et al.*, Plasma Phys. Control. Fusion **44**, A123 (2002).
[7] K.H. Burrell, *et al.*, Plasma Phys. Control. Fusion **44**, A253 (2002).
[8] C.J. Lasnier, *et al.*, accepted for publication in J. Nucl. Mater. (2002).
[9] T.A. Casper, *et al.*, 29th EPS Conf. on Plasma Phys. and Contr. Fusion, Montreux, Switzerland, ECA Vol. **26B**, P-2.065 (2002).
[10] H. Zohm, these proceeding, paper OV/2-1 (2002).
[11] T.A. Casper, *et al.*, 27th EPS Conf. on Plasma Phys. and Contr. Fusion, Budapest, Hungary, ECA Vol. **24B**, 1545 (2000).
[12] B.W. Rice, *et al.*, Rev. Sci. Instrum **70**, 815 (1999).
[13] D.R. Baker., *et al.*, Phys. Plasmas **8**, 1565 (2001).
[14] R. Neu, *et al.*, Plasma Phys. Control. Fusion **44**, 811 (2002).
[15] R.A. Hulse, Nucl. Technologies/Fusion **3**, 259 (1983).
[16] S.P. Schissel *et al.*, Phys. Fluids B **1**, 1843 (1989).
[17] R.J. Hawryluk, in *Proc. of the Course in Physics Close to Thermonuclear Conditions*, Varenna, 1979, Vol. I, (CEC, Brussels, 1980) p.19.
[18] R.E. Waltz, private communication (2002).
[19] R.E. Waltz, *et al.*, Phys. Plasmas **4**, 2482 (1997).
[20] T.L. Rhodes, *et al.*, Phys. Plasmas **9**, 2141 (2002).
[21] T.L. Rhodes, *et al.*, these proceeding, paper EX/C4-1Rb (2002).
[22] L. Zeng, *et al.*, accepted for publication in Rev. Sci. Instrum. (2002).